



High performance infrared photodetectors up to 2.8 μm wavelength based on lead selenide colloidal quantum dots

M. THAMBIDURAI,¹ YOUNGJIN JANG,² ARTHUR SHAPIRO,² GAO YUAN,¹ HU XIAONAN,¹ YU XUECHAO,¹ QI JIE WANG,¹ EFRAT LIFSHITZ,² HILMI VOLKAN DEMIR,^{1,3,4} AND CUONG DANG^{1,5}

¹LUMINOUS! Centre of Excellence for Semiconductor Lighting and Displays, Centre for OptoElectronics and Biophotonics (COEB), School of Electrical and Electronic Engineering, The Photonics Institute (TPI), Nanyang Technological University, 50 Nanyang Avenue, 639798, Singapore

²Schulich Faculty of Chemistry, Solid State Institute and Russell Berrie Nanotechnology Institute, Technion, Haifa 32000, Israel

³Department of Electrical and Electronics Engineering, Department of Physics, UNAM—Institute of Materials Science and Nanotechnology, Bilkent University, Ankara 06800, Turkey

⁴hvdemir@ntu.edu.sg

⁵hcdang@ntu.edu.sg

Abstract: The strong quantum confinement effect in lead selenide (PbSe) colloidal quantum dots (CQDs) allows to tune the bandgap of the material, covering a large spectral range from mid- to near infrared (NIR). Together with the advantages of low-cost solution processability, flexibility and easy scale-up production in comparison to conventional semiconductors especially in the mid- to near infrared range, PbSe CQDs have been a promising material for infrared optoelectronic applications. In this study, we synthesized monodisperse and high purity PbSe CQDs and then demonstrated the photodetectors working at different wavelengths up to 2.8 μm . Our high quality PbSe CQDs show clear multiple excitonic absorption peaks. PbSe CQD films of different thicknesses were deposited on interdigitated platinum electrodes by a simple drop casting technique to make the infrared photodetectors. At room temperature, the high performances of our PbSe CQD photodetectors were achieved with maximum responsivity, detectivity and external quantum efficiency of 0.96 A/W, 8.13×10^9 Jones and 78% at 5V bias. Furthermore, a series of infrared LEDs with a broad wavelength range from 1.5 μm to 3.4 μm was utilized to demonstrate the performance of our fabricated photodetectors with various PbSe CQD film thicknesses.

© 2017 Optical Society of America

OCIS codes: (250.0250) Optoelectronics; (040.5160) Photodetectors; (160.4236) Nanomaterials; (300.6340) Spectroscopy, infrared; (160.6000) Semiconductor materials.

References and links

1. G. Zaiats, A. Shapiro, D. Yanover, Y. Kauffmann, A. Sashchiuk, and E. Lifshitz, "Optical and electronic properties of nonconcentric PbSe/CdSe colloidal quantum dots," *J. Phys. Chem. Lett.* **6**(13), 2444–2448 (2015).
2. A. Teitelboim, N. Meir, M. Kazes, and D. Oron, "Colloidal double quantum dots," *Acc. Chem. Res.* **49**(5), 902–910 (2016).
3. X. Yang, P. L. Hernandez-Martinez, C. Dang, E. Mutlugun, K. Zhang, H. V. Demir, and X. W. Sun, "Electroluminescence efficiency enhancement in quantum dot light-emitting diodes by embedding a silver nanoisland layer," *Adv. Optical Mater.* **3**(10), 1439–1445 (2015).
4. Z. Soran-Erdem, T. Erdem, P. L. Hernandez-Martinez, M. Z. Akgul, N. Gaponik, and H. V. Demir, "Macrocrystals of colloidal quantum dots in anthracene: exciton transfer and polarized emission," *J. Phys. Chem. Lett.* **6**(9), 1767–1772 (2015).
5. X. Wang, G. I. Koleilat, J. Tang, H. Liu, I. J. Kramer, R. Debnath, L. Brzozowski, D. Aaron, R. Barkhouse, L. Levina, S. Hoogland, and E. H. Sargent, "Tandem colloidal quantum dot solar cells employing a graded recombination layer," *Nat. Photonics* **5**(8), 480–484 (2011).
6. O. E. Semonin, J. M. Luther, S. Choi, H.-Y. Chen, J. Gao, A. J. Nozik, and M. C. Beard, "Peak external photocurrent quantum efficiency exceeding 100% via MEG in a quantum dot solar cell," *Science* **334**(6062), 1530–1533 (2011).

7. L. E. Bru, "Electron-electron and electron-hole interactions in small semiconductor crystallites: the size dependence of the lowest excited electronic state," *J. Chem. Phys.* **80**(9), 4403–4409 (1984).
8. A. Sashchiuk, D. Yanover, A. Rubin-Brusilovski, G. I. Maikov, R. K. Capek, R. Vaxenburg, J. Tilchin, G. Zaiats, and E. Lifshitz, "Tuning of electronic properties in IV-VI colloidal nanostructures by alloy composition and architecture," *Nanoscale* **5**(17), 7724–7745 (2013).
9. G. Xiao, Y. Wang, J. Ning, Y. Wei, B. Liu, W. W. Yu, G. Zou, and B. Zou, "Recent advances in IV-VI semiconductor nanocrystals: synthesis, mechanism and applications," *RSC Advances* **3**(22), 8104–8130 (2013).
10. R. D. Schaller, M. A. Petruska, and V. I. Klimov, "Tunable near-infrared optical gain and amplified spontaneous emission using PbSe nanocrystals," *J. Phys. Chem. B* **107**(50), 13765–13768 (2003).
11. J. E. Murphy, M. C. Beard, A. G. Norman, S. P. Ahrenkiel, J. C. Johnson, P. Yu, O. I. Mičić, R. J. Ellingson, and A. J. Nozik, "PbTe colloidal nanocrystals: synthesis, characterization, and multiple exciton generation," *J. Am. Chem. Soc.* **128**(10), 3241–3247 (2006).
12. S. J. Heo, S. Yoon, S. H. Oh, D. H. Yoon, and H. J. Kim, "Influence of high-pressure treatment on charge carrier transport in PbS colloidal quantum dot solids," *Nanoscale* **6**(2), 903–907 (2014).
13. Y. Pan, H. Bai, L. Pan, Y. Li, M. C. Tamargo, M. Sohel, and J. R. Lombardi, "Size controlled synthesis of monodisperse PbTe quantum dots: using oleylamine as the capping ligand," *J. Mater. Chem.* **22**(44), 23593–23601 (2012).
14. C. Li, T. Bai, F. Li, L. Wang, X. Wu, L. Yuan, Z. Shi, and S. Feng, "Growth orientation, shape evolution of monodisperse PbSe nanocrystals and their use in optoelectronic devices," *CrystEngComm* **15**(3), 597–603 (2013).
15. A. Rogalski, *Infrared Detectors* (CRC Press, 2010).
16. X. Gong, M. Tong, Y. Xia, W. Cai, J. S. Moon, Y. Cao, G. Yu, C. L. Shieh, B. Nilsson, and A. J. Heeger, "High-detectivity polymer photodetectors with spectral response from 300 nm to 1450 nm," *Science* **325**(5948), 1665–1667 (2009).
17. L. B. Luo, H. Hu, X.-H. Wang, R. Lu, Y. F. Zou, Y.-Q. Yu, and F.-X. Liang, "A graphene/GaAs near-infrared photodetector enabled by interfacial passivation with fast response and high sensitivity," *J. Mater. Chem. C Mater. Opt. Electron. Devices* **3**(18), 4723–4728 (2015).
18. J. Saghaei, A. Fallahzadeh, and T. Saghaei, "Vapor treatment as a new method for photocurrent enhancement of UV photodetectors based on ZnO nanorods," *Sens. Actuators A Phys.* **247**, 150–155 (2016).
19. S. Keuleyan, J. Kohler, and P. Guyot-Sionnest, "Photoluminescence of Mid-Infrared HgTe Colloidal Quantum Dots," *J. Phys. Chem. C* **118**(5), 2749–2753 (2014).
20. X. Zhou, L. Gan, Q. Zhang, X. Xiong, H. Li, Z. Zhong, J. Han, and T. Zhai, "High performance near-infrared photodetectors based on ultrathin SnS nanobelts grown via physical vapor deposition," *RSC Advances* **5**, 54109–54114 (2015).
21. G. Wei, Z. Lu, Y. Cai, and C. Sui, "CuPc/C60 heterojunction photodetector with near-infrared spectral response," *Mater. Lett.* **201**, 137–139 (2017).
22. X. X. Gong, G. T. Fei, W. B. Fua, B. N. Zhonga, X. D. Gao, and L. D. Zhang, "Metal-semiconductor-metal infrared photodetector based on PbTe nanowires with fast response and recovery time," *Appl. Surf. Sci.* **404**, 7–11 (2017).
23. H. Tan, C. Fan, L. Ma, X. Zhang, P. Fan, Y. Yang, W. Hu, H. Zhou, X. Zhuang, X. Zhu, and A. Pan, "Single-crystalline InGaAs nanowires for room-temperature high-performance near-infrared photodetectors," *Nano-Micro Lett.* **8**(1), 29–35 (2016).
24. X. Dai, S. Zhang, Z. Wang, G. Adamo, H. Liu, Y. Huang, C. Couteau, and C. Soci, "GaAs/AlGaAs nanowire photodetector," *Nano Lett.* **14**(5), 2688–2693 (2014).
25. J. Miao, W. Hu, N. Guo, Z. Lu, X. Liu, L. Liao, P. Chen, T. Jiang, S. Wu, J. C. Ho, L. Wang, X. Chen, and W. Lu, "High-responsivity graphene/InAs nanowire heterojunction near-infrared photodetectors with distinct photocurrent on/off ratios," *Small* **11**(8), 936–942 (2015).
26. L. B. Luo, H. Hu, X. H. Wang, R. Lu, Y. F. Zou, Y. Q. Yu, and F. X. Liang, "graphene/GaAs near-infrared photodetector enabled by interfacial passivation with fast response and high sensitivity," *J. Mater. Chem. C Mater. Opt. Electron. Devices* **3**(18), 4723–4728 (2015).
27. U. Nithiyanantham, M. F. Ozaydin, A. S. Tazebay, and S. Kundu, "Low temperature formation of rectangular PbTe nanocrystals and their thermoelectric properties," *New J. Chem.* **40**(1), 265–277 (2016).
28. E. V. Ushakova, A. P. Litvin, P. S. Parfenov, A. V. Fedorov, M. Artemyev, A. V. Prudnikau, I. D. Rukhlenko, and A. V. Baranov, "Anomalous size-dependent decay of low-energy luminescence from PbS quantum dots in colloidal solution," *ACS Nano* **6**(10), 8913–8921 (2012).
29. J. J. Urban, D. V. Talapin, E. V. Shevchenko, and C. B. Murray, "Self-assembly of PbTe quantum dots into nanocrystal superlattices and glassy films," *J. Am. Chem. Soc.* **128**(10), 3248–3255 (2006).
30. B. Wang, H. Xia, Z. Zhang, J. Yang, R. Patterson, S. Huang, S. Shrestha, and G. Conibeer, "Ab initio calculation of halide ligand passivation on PbSe quantum dot facets," *RSC Advances* **6**(106), 104699 (2016).
31. Z. Huang, G. Zhai, Z. Zhang, C. Zhang, Y. Xia, L. Lian, X. Fu, D. Zhang, and J. Zhang, "Low cost and large scale synthesis of PbS quantum dots with hybrid surface passivation," *CrystEngComm* **19**(6), 946–951 (2017).
32. Z. Lin, Z. Yang, P. Wang, G. Wei, A. He, W. Guo, and M. Wang, "Schottky-ohmic converted contact, fast-response, infrared PbTe photodetector with stable photoresponse in air," *RSC Advances* **6**(109), 107878 (2016).
33. K. Qiao, H. Deng, X. Yang, D. Dong, M. Li, L. Hu, H. Liu, H. Song, and J. Tang, "Spectra-selective PbS quantum dot infrared photodetectors," *Nanoscale* **8**(13), 7137–7143 (2016).

34. S. A. McDonald, G. Konstantatos, S. Zhang, P. W. Cyr, E. J. D. Klem, L. Levina, and E. H. Sargent, "Solution-processed PbS quantum dot infrared photodetectors and photovoltaics," *Nat. Mater.* **4**(2), 138–142 (2005).
35. E. J. D. Klem, C. Gregory, D. Temple, and J. Lewis, "PbS colloidal quantum dot photodiodes for low-cost SWIR sensing," *Proc. SPIE* **9451**, 945104 (2015).
36. H. Choi, J. H. Song, J. Jang, X. D. Mai, S. Kim, and S. Jeong, "High performance of PbSe/PbS core/shell quantum dot heterojunction solar cells: short circuit current enhancement without the loss of open circuit voltage by shell thickness control," *Nanoscale* **7**(41), 17473–17481 (2015).
37. L. Yan, X. Shen, Y. Zhang, T. Zhang, X. Zhang, Y. Feng, J. Yin, J. Zhao, and W. W. Yu, "Near-infrared light emitting diodes using PbSe quantum dots," *RSC Advances* **5**(67), 54109–54114 (2015).
38. M. K. Jana, B. Murali, S. B. Krupanidhi, K. Biswas, and C. N. R. Rao, "Fabrication of large-area PbSe films at the organic–aqueous interface and their near-infrared photoresponse," *J. Mater. Chem. C Mater. Opt. Electron. Devices* **2**(31), 6283–6289 (2014).
39. L. Etgar, E. Lifshitz, and R. Tannenbaum, "Hierarchical conjugate structure of γ -Fe₂O₃ nanoparticles and PbSe quantum dots for biological applications," *J. Phys. Chem. C* **111**(17), 6238–6244 (2007).
40. H. E. Romero, and M. Drndic, "Coulomb blockade and hopping conduction in PbSe quantum dots," *Phys. Rev. Lett.* **95**, 156801 (2005).
41. Z. Yang, M. Wang, Y. Shi, X. Song, Z. Lin, Z. Ren, and J. Bai, "The impact of chemical treatment on optical and electrical characteristics of multipod PbSe nanocrystal films," *J. Mater. Chem.* **22**(39), 21009–21016 (2012).
42. G. Sarasqueta, K. R. Choudhury, and F. So, "Effect of Solvent Treatment on Solution-Processed Colloidal PbSe Nanocrystal Infrared Photodetectors," *Chem. Mater.* **22**(11), 3496–3501 (2010).
43. M. Sulaman, S. Yang, A. Bukhtiar, C. Fu, T. Song, H. Wang, Y. Wang, H. Bo, Y. Tang, and B. Zou, "High performance solution-processed infrared photodetector based on PbSe quantum dots doped with low carrier mobility polymer poly(Nvinylcarbazole)," *RSC Advances* **6**(50), 44514–44521 (2016).
44. D. Yanover, R. K. Capek, A. Rubin-Brusilovski, R. Vaxenburg, N. Grumbach, G. I. Maikov, O. Solomeshch, A. Sashchiuk, and E. Lifshitz, "Small-sized PbSe/PbS core/shell colloidal quantum dots," *Chem. Mater.* **24**(22), 4417–4423 (2012).
45. A. Shapiro, Y. Jang, A. Rubin-Brusilovski, A. K. Budniak, F. Horani, A. Sashchiuk, and E. Lifshitz, "Tuning optical activity of IV–VI colloidal quantum dots in the short-wave infrared (SWIR) spectral regime," *Chem. Mater.* **28**(17), 6409–6416 (2016).
46. D. Yu, C. Wang, and P. Guyot-Sionnest, "n-Type conducting CdSe nanocrystal solids," *Science* **300**(5623), 1277–1280 (2003).
47. D. Zhang, G. Zhai, J. Zhang, L. Yuan, X. Miao, S. Zhu, and Y. Wang, "Growth orientation and shape evolution of colloidal lead selenide nanocrystals with different shapes," *CrystEngComm* **12**(10), 3243–3248 (2010).
48. Y. Chen, G. Zhang, Z. Dong, J. Wei, J.-L. Zhu, and J.-L. Sun, "Fabrication of Au nanoparticle/double-walled carbon nanotube film/TiO₂ nanotube array/Ti heterojunctions with low resistance state for broadband photodetectors," *Physica B* **508**, 1–6 (2017).
49. S. C. Dhanabalan, J. S. Ponraj, H. Zhang, and Q. Bao, "Present perspectives of broadband photodetectors based on nanobelts, nanoribbons, nanosheets and the emerging 2D materials," *Nanoscale* **8**(12), 6410–6434 (2016).
50. D. Zare-Hossein-abadi, A. Ershad-Langroudi, A. Rahimi, and S. Afsar, "Photo-generated activities of nanocrystalline TiO₂ thin films," *J. Inorg. Organomet. Polym. Mater.* **20**(2), 250–257 (2010).
51. A. K. Seferlis and S. G. Neophytides, "Photoelectrocatalytic electricity and/or H₂ production from alcohols: the effect of TiO₂ film Thickness," *J. Electrochem. Soc.* **158**(2), H183–H189 (2011).
52. W. Y. Zhang, S. Zhong, L. J. Sun, and Z. X. Fu, "Dependence of photovoltaic property of ZnO/Si heterojunction solar cell on thickness of ZnO films," *Chin. Phys. Lett.* **25**(5), 1829–1831 (2008).
53. N. Naseri, S. Yousefzadeh, E. Daryaei, and A. Z. Moshfegh, "Photoresponse and H₂ production of topographically controlled PEG assisted sol–gel WO₃ nanocrystalline thin films," *Int. J. Hydrogen Energy* **36**(21), 13461–13472 (2011).
54. J. Nissfolk, K. Fredin, J. Simiyu, L. Haggman, A. Hagfeldt, and G. Boschloo, "Interpretation of small-modulation photocurrent transients in dye-sensitized solar cells – A film thickness study," *J. Electroanal. Chem.* **646**(1–2), 91–99 (2010).
55. R. A. Pala, A. J. Leenheer, M. Lichterman, H. A. Atwater, and N. S. Lewis, "Measurement of minority-carrier diffusion lengths using wedge-shaped semiconductor photoelectrode," *Energy Environ. Sci.* **7**(10), 3424–3430 (2014).
56. J. D. Vincent, S. Hodges, J. Vampola, M. Stegall, and G. Pierce, *Fundamentals of Infrared and Visible Detector Operation and Testing* (John Wiley & Sons, 2015).

1. Introduction

Colloidal quantum dots (CQDs) have been studied extensively due to their attractive optoelectronic properties such as high luminescence efficiency, large dipole moment, strong light absorption, good photo-stability, and multiple electron hole pair generation [1–4]. More importantly, the strong quantum confinement effect allows us to tailor the energy band gap of these materials by controlling their size in a cost-effective wet chemical synthesis [5–7]. These advantages bring CdSe-based CQDs to a competitive market of lighting and display

technology today. The research on lead based chalcogenide (PbTe, PbS, and PbSe) CQDs for infrared applications has also received much scientific and technological attention because of the possibility to tune the bandgap in the infrared wavelength range [8–14]. Infrared (IR) photodetectors are important components in many different areas such as thermal imaging, telecommunication, medical diagnostics, missile guidance, astronomy and environment sensing [15–20]. Short-wave IR (SWIR) research with various materials has been attracting a lot of attentions [21,22]. For examples, Graphene/III-V semiconductor nanowire heterojunction near-infrared photodetectors [23–25] have been reported with a photoresponsivity of 0.5 A/W in the infrared region ($\lambda = 1000$ nm); bilayer graphene/gallium arsenide Schottky junction [26] shows the photo- responsivity and detectivity of 0.005 A/W and 2.88×10^{11} (Jones). After the early literatures about lead chalcogenide CQD material developments, structural and optical properties as well as the surface morphology of their thin film [27–31], the photodetectors based on lead chalcogenide CQDs have been reported for a limited spectrum in visible and near infrared region. For example, Lin et al. [32] investigated the infrared PbTe CQD photodetector characteristics with inorganic halide ligand treatment (tetrabutylammonium iodide) and reported that the responsivity at 1064 nm wavelength was up to 1.9 mA/W with fine tuning of CQD film thickness (91 nm). Qiao et al. [33] studied PbS CQD infrared photodetectors and reported that responsivity and detectivity were 8.2 mA/W, 7.2×10^{10} Jones for 390 nm and 15.6 mA/W, 1.3×10^{11} Jones for 930 nm light detection, respectively. McDonald et al. [34] studied solution processed PbS CQD infrared photodetectors and reported the responsivity as 3.1 mA/W for 975 nm illumination. These PbS CQD photodetectors for near infrared spectrum only reach around 1.7 μ m wavelength [35], the transition range between NIR and SWIR.

Among the lead based chalcogenide family, lead selenide (PbSe) CQDs have received more attention in not only photodetectors but also many infrared optoelectronic applications like solar cells, light emitting diodes, etc [36–38]. The bulk PbSe semiconductor has a narrow energy band gap of 0.27 eV at room temperature; it exhibits cubic crystal structure (space group Fm3m), large exciton Bohr radius (46 nm), small effective masses for both electrons and holes, and a large dielectric constant [39–41]. Sarasqueta et al. [42] studied the roles of solvent treatment on infrared photodetectors based on PbSe nanocrystals. Sulaman et al. [43] investigated the behavior of solution-processed infrared photodetectors (field-effect transistor devices) based on PbSe CQDs doped with low carrier mobility polymer poly (N-vinylcarbazole); and the reported responsivity was in the range of 0.0266 to 2.93 A/W for 980 nm illumination. With small band gap of corresponding bulk material and very large exciton Bohr radius, PbSe CQDs have great potentials to extend the spectral range of photodetection close to mid-IR region [44]. In the present work, we report about high performance photodetectors at a broad spectral range, for the first time, up to 2.8 μ m based on our high quality, monodisperse PbSe CQDs. The synthesized PbSe CQDs were studied by high resolution transmission electron microscopy (HRTEM), x-ray diffraction (XRD), Fourier transform infrared (FTIR) spectroscopy and absorbance spectroscopy. We deposited thin films of synthesized PbSe CQDs on the patterned interdigitated platinum electrodes by a drop casting method to create photodetectors. These photodetectors with different thicknesses of the PbSe CQD film were studied and optimized in detail for the best performance. We achieved the highest responsivity and external quantum efficiency of 0.96 A/W and 78% for PbSe CQD near-infrared photodetectors. The photocurrent responses were recorded as a function of bias voltage using infrared LED illuminations with wavelengths of up to 2.8 μ m.

2. Experiments

2.1 Synthesis of PbSe CQDs

Lead (II) oxide (PbO; 99.999%), selenium (Se; 99.99%), n-hexadecane (HDC; 99%) and oleic acid (OA; 90%) were purchased from Sigma-Aldrich. Ammonium chloride (A.C.S. grade) was purchased from Spectrum Chemicals. Trioctylphosphine (TOP; 97%) and

diphenylphosphine (DPP; 99%) were purchased from Strem. Methanol (absolute) and toluene (analytical) were purchased from Bio-Lab Ltd. Acetone (absolute) was purchased from Gadot. These chemicals were used without further purification.

The PbSe CQDs were synthesized by modifying the procedure developed by Lifshitz and associates [44,45]. The reaction mixture containing 0.8 mmol of PbO, 2.4 mmol of OA, and HDC (the total mass of reaction mixture was 8 g) was heated to 100 °C for 1 h under vacuum. Then, the mixture solution was heated to 180 °C under nitrogen. Next, the selenium precursor solution containing 0.8 ml of 1 M TOPSe, 1.6 mmol of DPP, 6.4 mmol of TOP, and HDC (the total volume of stock solution was 4 mL) was rapidly injected into the Pb oleate solution under nitrogen. The temperature decreased to 160 °C and the reaction mixture was kept until appropriate growth was obtained. Afterwards, the reaction vessel was allowed to cool down to 60 °C and then 1 mL of 0.2 M ammonium chloride solution (in methanol) was added to obtain better surface passivation by halide treatment. The mixture solution was the CQDs and they were isolated by centrifuging using methanol and acetone. The purification process was repeated twice. Final precipitate was dried and then re-dissolved in toluene for further usage.

2.2 Device fabrication

The patterned interdigitated platinum electrodes on glass substrates were cleaned using acetone, isopropanol, ethanol and deionized water in a sonication bath before the PbSe CQDs film deposition. The 20 mg of PbSe CQDs was dissolved in 1 ml of hexane. Prepared solution was deposited on interdigitated platinum electrode substrates by drop casting method. After drying, the films were dipped for 1 minute in a solution of ethanol and 5% ethanedithiol and then it was rinsed using ethanol and dried at 60 °C. Ligand exchange reduces the barrier between the particles [46], readily improves the conductivity by 3 to 4 orders of magnitude in our samples. The process was repeated for thicker film formation.

2.3 Characterization

The x-ray diffraction pattern of the PbSe CQDs samples was recorded on Shimazu (XRD-6000) diffractometer with CuK α radiation (1.54 Å). The high resolution transmission electron microscopy (HRTEM) images of the PbSe CQDs were recorded using JEOL JEM 2010 electron microscope. The absorption spectra of the PbSe CQDs samples were measured using Perkin Elmer Lambda 950 UV-Vis-NIR spectrophotometer. Fourier transform infrared (FTIR) spectra of the samples were recorded by Shimadzu IR Prestige-21 FTIR spectrophotometer. The film thicknesses were measured using a surface profilometer to be 500 nm, 900 nm and 1400 nm. The current-voltage (I-V) characteristics of the PbSe CQDs devices were measured using a Keithley-2450 source meter unit with 1.520 μ m continuous wave laser illumination. The photocurrent responses were measured as a function of bias voltage using lock-in amplifier with various LED from 1.5 μ m to 3.4 μ m illuminations. All the characterization experiments were done at room temperature.

3. Results and discussion

The grain size and crystal structure of the PbSe CQDs have been studied by HRTEM and XRD techniques as shown in Fig. 1. The TEM image (Fig. 1(a)) of PbSe CQDs shows that all the nanoparticles are of spherical shape with uniform size. The size distribution and the corresponding Gaussian curve fitting for the synthesized PbSe CQDs are shown in Fig. 1(b), in which the results were analyzed from more than 100 nanoparticles. The average grain size of PbSe CQDs is found to be 8.0 nm. Figure 1(c) shows the HRTEM image of PbSe CQDs. The lattice spacing has been calculated using the fringes as 3.04 Å and this corresponds to the (200) plane of cubic PbSe structure. Figure 1(d) shows the x-ray diffraction pattern of PbSe CQDs film. The diffraction peaks correspond to (111), (200), (220), (311), (222), (400), (420) and (422) planes of cubic phase PbSe. The lattice constant (a) is calculated based on the XRD data to be $a = 6.12$ Å, which matches with the standard JCPDS data. No other impurity phase

was detected, implying that the prepared PbSe CQDs are of high purity. The crystal size of PbSe CQDs has been determined from full width at half maximum (FWHM) peak using Scherrer's formula $D = K\lambda / \beta \cos(\theta)$ where, θ , λ , K , β and D are angle of diffraction, x-ray wavelength, constant ($K = 0.94$), FWHM of the diffraction peak and grain size. The calculated grain size by X-ray diffraction pattern is 8.5 nm, which is in a good agreement with HRTEM results.

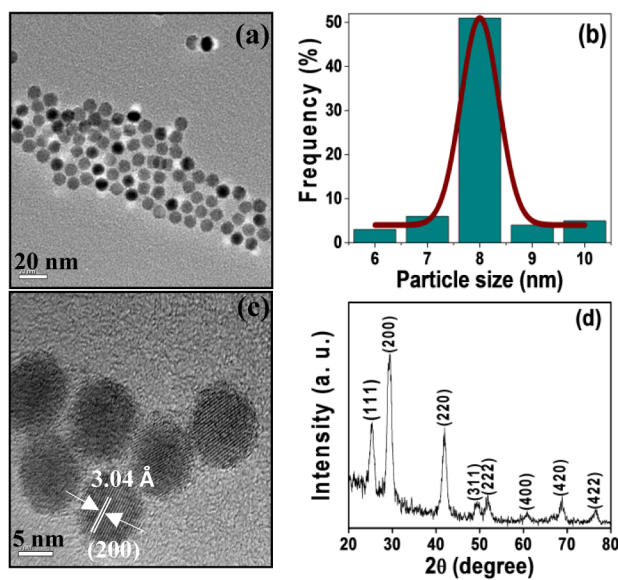


Fig. 1. Characterization of PbSe CQDs. (a) The TEM image of PbSe CQDs shows the monodisperse nanoparticles. (b) Histogram of the PbSe nanoparticle size distribution. (c) The HRTEM of PbSe nanoparticles. (d) The x-ray diffraction pattern of PbSe nanoparticles.

Figure 2(a) presents the absorbance spectra of the typical PbSe CQD films calculated from transmission spectra, which were measured by two different methods: wavelength scanning monochromatic light and FTIR. The two methods cover different ranges of wavelength with significant overlap in our interested spectrum region. Near-infrared absorption spectra exhibit discrete excitonic features in both approaches, revealing the presence of high-quality, monodisperse PbSe semiconductor nanocrystals. Two independent experiments show the same two absorbance peaks at 2440 nm (0.50 eV), 1940 nm (0.63 eV) which are the third and the second exciton peaks of our PbSe CQDs, respectively. While the first excitonic transition appears at 2780 nm (0.44 eV) in the FTIR spectrum, showing the semiconductor bandgap at short-wavelength infrared and close to mid-infrared region. The wavelength scanning monochromatic light approach, which cannot show the first exciton peak because of the limited light intensity at long wavelength, reveals some features around 1490 nm (0.83 eV) which is again out of range for FTIR method. Figure 2(b) presents the absorbance spectrum of CQD solution where the scattering effect is significantly reduced in comparison with the film counterpart. Therefore the signal is cleaner, and extra exciton peaks are revealed in addition to the ones observed in the thin film. The results demonstrate our high quality, monodispersed PbSe CQDs. It should be noted that two sharp peaks present at 3425 nm and 3505 nm in FTIR measurement are associated with vibrational modes of the ligand on the surface of PbSe CQDs. The absorption peaks of our PbSe CQDs are blue shifted when compared to the bandgap value of bulk PbSe (4430 nm or 0.27 eV). This clearly indicates the nature of monodisperse PbSe nanoparticles with a strong quantum confinement effect [47].

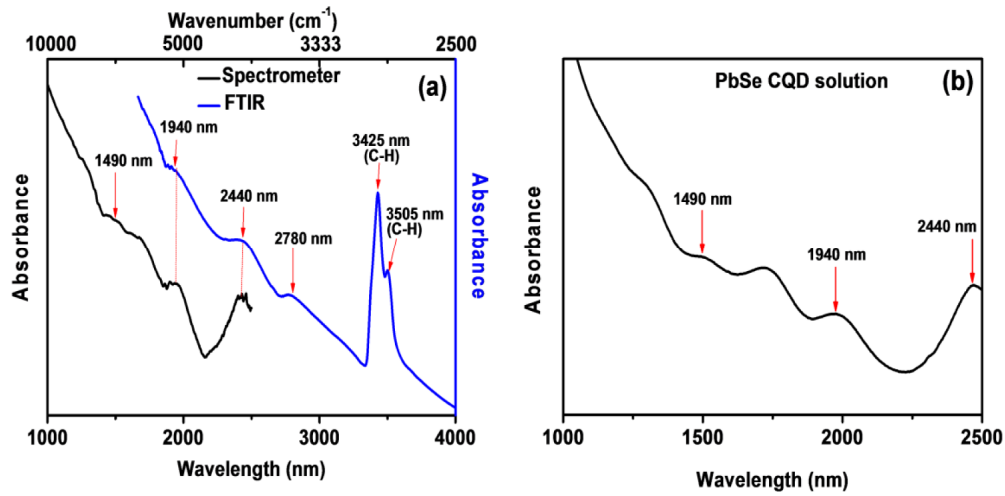


Fig. 2. (a) Absorbance spectra of PbSe CQD film measured by single wavelength scanning spectrometer (black color) and FTIR (blue color). (b) Absorbance spectrum of PbSe CQD solution

We utilized our PbSe CQDs in the infrared photodetector with photoconductivity device configuration as shown in Fig. 3(a). The interdigitated platinum electrodes on glass substrates (ref.G-IDEPT5) were purchased from Dropsens, Spain. The electrode gap, length, and number of digits are 5 μm , 6760 μm , and 250×2 , respectively. We systematically investigated the effect of the PbSe thin film thickness on the performance of our photodetector devices. Current-voltage (I-V) characteristics of our PbSe CQD photodetectors under ambient conditions in the dark and laser light illumination (1.52 μm) with various film thicknesses (500 nm, 900 nm and 1400 nm) are shown in Fig. 3(b). The thicker films show better conductivity (higher current) as usual and the resistances of the three devices are in the range of 200 Ω to 1 k Ω . Under laser light illumination from the top of devices, the illuminated current is greater than the dark current for every bias voltage. The difference between the bright (I_{light}) and dark (I_{dark}) current is the photocurrent. With normalization to the laser

intensity (P_{in}), we get the responsivity $R = \frac{(I_{\text{light}} - I_{\text{dark}})}{P_{\text{in}}}$ of our photodetector devices [48]

at different bias voltage as presented in Fig. 3(c). The responsibility increases monotonically with bias voltage but the role of PbSe CQD film thickness is clearly shown in Fig. 3(c). The highest responsibility was achieved as 0.96 A/W at 5 Volt bias in the sample with 900 nm CQD film. The thinner (500 nm) and thicker (1400 nm) CQD films show the responsibilities of 0.48 A/W and 0.33 A/W, respectively.

The external quantum efficiency (EQE) of our photodetectors can be calculated from responsibility by the following equation [49] $EQE = \frac{hcR}{q\lambda}$ where, h , c , and λ are Planck's constant, the velocity of light, and the excitation wavelength, respectively. The EQE presents ratio of extracted charge number and the incident photon number. By increasing the bias voltage, we can increase the extraction efficiency and therefore increase the EQE as seen in Fig. 3(c) for all the samples. The maximum EQE of 78% was achieved at 5V with the sample of 900 nm PbSe CQD film while the EQE values for thinner (500 nm) and thicker (1400 nm) samples were 40% and 27%, respectively. There are two factors that affect the EQE or responsibility: absorption of incident photons and extraction of generated charge carriers. Thicker film creates more photo-generated charge carriers owing to their higher absorption coefficient. Therefore, the photocurrent increases with film thickness initially. The extraction of these carriers is determined by the distance from the carriers to the electrodes, the electric

field (ξ) between the electrodes, the lifetime (τ) and mobility (μ_e , μ_h) of photo-generated carriers (electrons, holes). The carrier drifting lengths ($l_{e,h} = \tau \xi \mu_{e,h}$) are the measure of how far the electrons and holes can travel before recombination. The photo-generated carrier concentration is the most on the top surface where the light shines to the devices, then decay exponentially at deeper layers. The electrodes are at the bottom of the samples, thus, the CQD film thickness generally determines the average path length of the generated carriers to the electrodes. When the thickness of the film is greater than the carrier drifting length, more electrons and holes are recombined before reaching the electrode surfaces [50–54], which would greatly reduce photocurrent in the thick PbSe CQD film device. The device responsivity demonstrated in our study indicates first an increase and then a decrease with the increase in film thickness; and this variation is in agreement with the experimental observations of Pala et al. [55]. In our study, we were using commercial interdigitated electrodes with fix gap of 5 μm which is much larger than the film thickness. However, it is worth to note that reducing the gap between electrodes would increase the extraction efficiency because of not only reducing the average carrier path length to electrodes but also increasing the electric field.

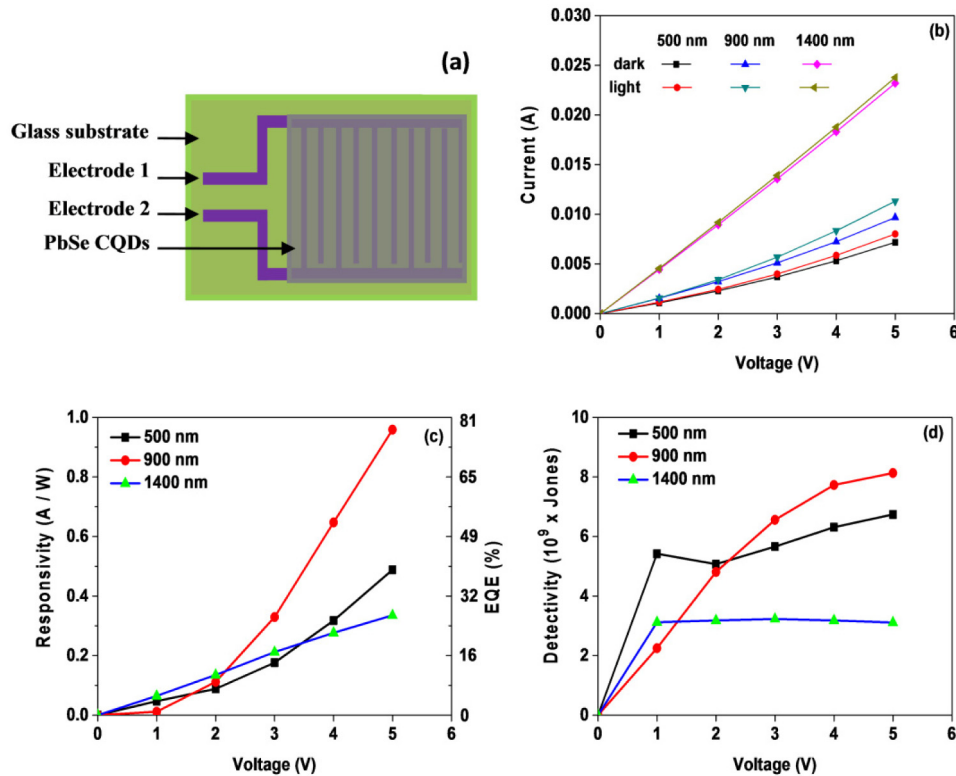


Fig. 3. (a) The schematic diagram of PbSe CQD photodetectors. (b) The current-voltage (I-V) characteristics of PbSe CQD photodetector device under ambient conditions in the dark and light illumination (1.52 μm). (c) The responsivity and EQE of our photodetector devices with different film thickness. (d) The detectivity as a function of bias voltage for our three devices.

For photoconductive devices, the noises such as generation-recombination (G-R) noise, Johnson noise or 1/f noise limit the detectivity. If, as expected, the G-R noise is the major contribution [16, 20, 38, 43], the specific detectivity (D^*) can be determined by the following

equation [56], $wD^* = \frac{R\sqrt{A}}{\sqrt{4qgI_{\text{dark}}}}$ here q is the electron charge (1.60×10^{-19} Coulombs), A is

effective area, and g is photocurrent gain. The photocurrent gain represents the ratio of collected charge carriers at the electrodes to the ones generated by photons in a time unit. For CQDs, we can assume that the internal quantum efficiency is 1, i.e. 1 e-h pair generated per photon. Thus photocurrent gain (g) is the device's EQE which depends on bias voltage as in Fig. 3(c). Figure 3(d) presents the devices' specific detectivity as a function of bias voltage. Increasing the bias voltage before photocurrent saturation will improve the detectivity. The highest detectivity values were found to be 6.74×10^9 Jones, 8.13×10^9 Jones, and 3.11×10^9 Jones for the devices of 500 nm, 900 nm, and 1400 nm PbSe CQD film thickness at 5V bias, respectively. The 1400 nm thickness sample with lowest responsivity and highest dark current shows the lowest detectivity.

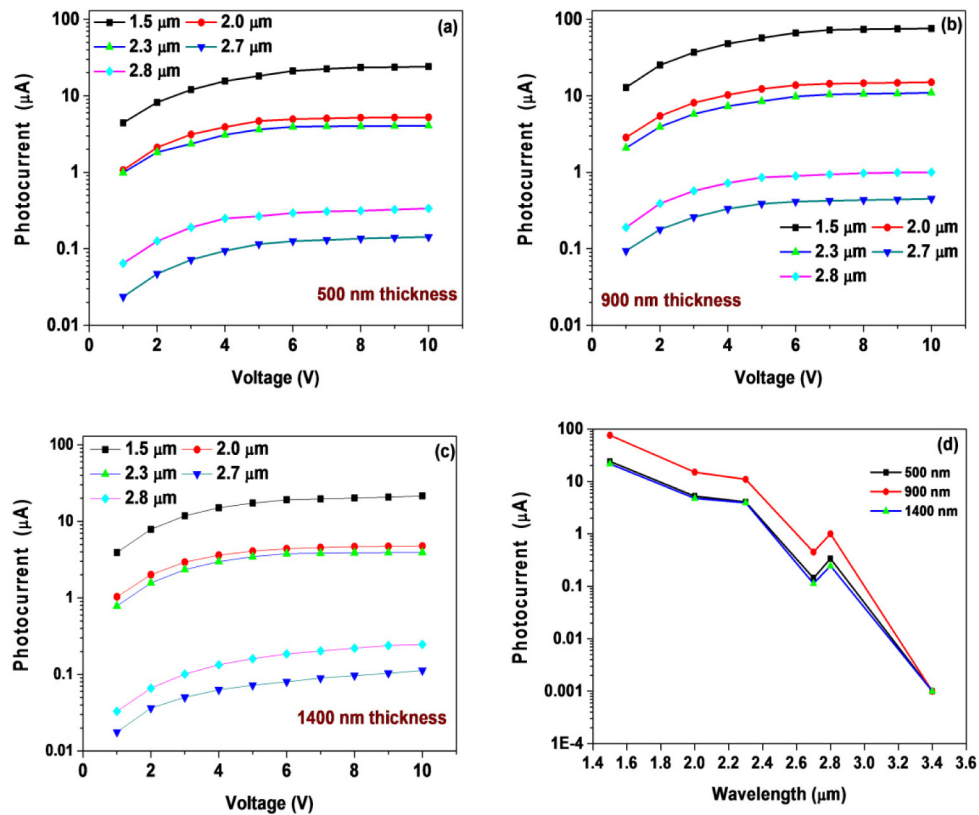


Fig. 4. Photocurrent-voltage characteristics of photodetectors under various LED illuminations with wavelength from 1.5 μm to 2.8 μm for PbSe CQD thickness of (a) 500 nm, (b) 900 nm and (c) 1400 nm. (d) The photocurrent of our three devices as a function of LED wavelength at the bias voltage of 10V.

We demonstrated our photodetector devices at longer wavelengths by utilizing a set of commercial LEDs (centre wavelength from 1.5 μm to 2.8 μm) as presented in Fig. 4. It is noted that the performance of present LEDs at these wavelengths are very poor with power in the range of μW and running in quasi-CW mode which is 1 kHz of square current (50% duty cycle). The quasi-CW mode operation of LEDs was used as modulated light sources for our lock-in detection technique. The photocurrent-voltage characteristics of PbSe CQD photodetector with three different thicknesses and under various LED light illuminations are

shown in Fig. 4(a)-4(c). The photocurrent is reported here as the peak-to-peak current in our lock-in detection technique. Again, the photocurrent is reaching the highest value for the sample with CQD film thickness of 900 nm. The photocurrents increase monotonically with bias voltage and then reach saturated levels around 6V. All the devices show the photocurrent response to the illumination light from 1.5 μm to 2.8 μm which is characteristics of PbSe CQD materials. Figure 4(d) summarizes the photocurrent as a function of LED wavelength for three samples at 10V bias. Our photocurrent measurement with 3.4 μm LED illumination did not show any signal rather than background noise ($\sim\text{nA}$) which is the last data point at 3.4 μm in the Fig. 4(d). While the absolute powers of LEDs were not measurable, their intensities monotonically decrease with increase of wavelength. The photocurrent peaks around 2.3 μm and 2.8 μm resemble the absorbance peaks of our PbSe CQD materials (Fig. 2).

4. Conclusions

In summary, we have successfully synthesized monodisperse and high purity PbSe CQDs and demonstrate their high performance for infrared photodetection. The responsivity of our photodetectors with respect to some LED wavelengths resembles the absorbance spectrum of our high quality PbSe CQD films with exciton peaks up to 2.8 μm . The device performance is dictated by the absorption of the PbSe CQD film and extraction of the photo-generated charge carriers. The former increases with film thickness while the latter is limited by carrier drifting length and therefore decreases with the increase of film thickness. Controlling the PbSe CQD film thickness is important to balance these two effect and achieve high performance photodetector devices. The highest responsivity and detectivity of our photodetectors are 0.96 A/W and 8.13×10^9 Jones, respectively for the device with 900 nm film thickness under 1.52 μm laser illumination. The obtained results indicate that the PbSe CQD material is a promising candidate for high performance photodetector at the infrared spectrum.

Funding

Nanyang Technological University (M4081482); Singapore National Research Foundation (NRF2015 NRF-CRP002-008); Singapore Ministry of Education (MOE2016-T2-1-128, RG70/15); Israel Council for Higher Education (872967); Volkswagen Stiftung (88116); Israel Ministry of Defence (4440665406); Israel Ministry of Trade (54662); Niedersachsen- Deutsche Technion Gesellschaft E.V (ZN2916).

Acknowledgments

We would like to thank the financial supports from NTU start-up grant (M4081482), Singapore National Research Foundation, Competitive Research Program (NRF2015 NRFCRP002-008), Singapore Ministry of Education Tier 1 Program (RG70/15) and Tier 2 Program (MOE2016-T2-1-128). Y. J., A. S. and E. L. acknowledge the financial support from the Israel Council for Higher Education-Focal Area Technology (Project No. 872967), the Volkswagen Stiftung (Project No.88116), the Israel Ministry of Defence (Project No. 4440665406), the Israel Ministry of Trade (Maymad Project No. 54662), the Niedersachsen-Deutsche Technion Gesellschaft E.V (Project No. ZN2916). The transmission electron microscopy imaging was performed at the Facility for Analysis, Characterization, Testing and Simulation (FACTS) at Nanyang Technological University, Singapore.